Available online at www.sciencedirect.com

ScienceDirect

journal homepage: www.elsevier.com/locate/he

Synthesis and characterization of Cu core Pt–Ru shell nanoparticles for the electro-oxidation of alcohols

Juan Manuel Sieben[*,1], *Vanina Comignani, Andrea E. Alvarez, Marta M.E. Duarte*[2]

Instituto de Ingeniería Electroquímica y Corrosión, Universidad Nacional del Sur, B8000CPB Bahía Blanca, Argentina

ARTICLE INFO

Article history:
Received 17 October 2013
Accepted 6 December 2013
Available online 4 January 2014

Keywords:
Core-shell nanoparticles
Carbon supported electrocatalysts
Methanol and ethanol electro-oxidation

ABSTRACT

Cu@Pt–Ru core–shell supported electrocatalysts have been synthesized by a two-step process via a galvanic displacement reaction. XRD diffraction and EDX analysis, and cyclic voltammetry measurements revealed the presence of nanoparticles composed by a Cu-rich Pt–Cu core surrounded by a Pt-rich Pt–Ru shell. Cyclic voltammetry and chronoamperometric measurements showed that as-synthesized core–shell materials exhibit superior catalytic activity towards methanol and ethanol electro-oxidation compared to a commercial Pt–Ru/C catalyst with higher Pt loading. This behavior can be associated with the lattice mismatch between the Pt-rich shell and the Cu rich core, which in turn produces lattice-strain, surface ligand effects and a large amount of surface defect sites. In addition, the core–shell electrodes displayed a better catalytic activity and lower onset potentials for ethanol oxidation than for methanol oxidation.

1. Introduction

Several companies in the world are presently working on direct alcohol fuel cells (DAFCs) because they are considered to be the most promising devices for use in power systems for mobile, stationary and portable applications. Methanol and ethanol have been generally proposed as the fuel for proton exchange membrane fuel cells (PEMFC) because they are liquids (allowing easy handling, storage and distribution) and have energy densities close to that of gasoline [1]. However, the high cost and scarcity of Pt, along with the deficient activity and selectivity of anode electrocatalysts at temperatures compatible with available membranes are the main obstacles that currently limit the massive commercialization of this technology [2–4]. Therefore, scientists have made numerous efforts to find a solution for these problems. In order to improve the selectivity and efficiency of platinum towards the electro-oxidation of alcohols, an optimized catalyst should be multifunctional and composed by Pt and one or several oxophilic elements such as Ru, Sn, Mo, W, Ni, Os, Pd, Co, Au and Rh [5–13]. In addition, the composition and structure of the catalysts, along with their long-term stability should also be taken into account [1,14]. However, the platinum loading in a PEMFC electrode is still high (0.5 mg cm^{-2}) and must be reduced to values below

* *Corresponding author*. Tel./fax: +54 291 4595182.
E-mail address: jmsieben@uns.edu.ar (J.M. Sieben).
[1] Member of CONICET, Argentina.
[2] Member of Comisión de Investigaciones Científicas de la Provincia de Buenos Aires.

0360-3199/$ – see front matter
http://dx.doi.org/10.1016/j.ijhydene.2013.12.064

0.3 mg cm^{-2} in order to diminish significantly the cost of fuel cells stacks and make them competitive with conventional energy technologies.

Recently, there has been an increasing focus on the synthesis of nanoparticles with a core–shell structure. Several groups have demonstrated that catalysts with core–shell architecture prepared by galvanic replacement or atomic layer deposition have high Pt utilization, extended service life and excellent electrochemical activity [15–21]. Adzic et al. have demonstrated that Pt monolayer electrocatalysts synthesized by the galvanic displacement of Cu monolayer on different metal or alloy cores exhibit an enhanced catalytic activity for oxygen reduction compared to that of Pt/C [15,22–24]. Chen et al. [20] and Yan et al. [25] have reported that the CO tolerance to poisoning and the catalytic activity of Ru@Pt and Au@Pt core–shell nanoparticles is improved with respect of Pt nanoparticles. The performance of the catalysts was found to be dependent on the crystalline structure of the core and the lattice strain at the core–shell interface. Recently, Xu and coworkers [26] have utilized the combination of a dealloying strategy and replacement reaction of $Cu_{25}Al_{75}$ alloy foils to prepare nanoporous core–shell structure with Pt(Pd)/Cu alloy shell and Cu(or Pt(Pd)/Cu alloy) core. The nanoporous core–shell structured composites exhibited greatly enhanced electrocatalytic activity and stability for the oxidation of methanol and acetic acid compared with Pt–Ru/C and Pd/C catalysts. Kaplan et al. [27] synthesized two core–shell, RuCore–PtShell and IrNiCore–PtRuShell catalysts of high Pt utilization and low noble metal loading, which had significantly better activity for methanol and ethylene glycol oxidation than one of the best commercially available Pt–Ru/C catalysts. In addition, Ammam and Easton [28] prepared Cu@Pt/C core–shell catalysts with high catalytic activity for ethanol electro-oxidation and good long-term stability.

The main objective of this work is evaluate the catalytic behavior of different Cu@Pt–Ru core–shell particles supported on a pretreated carbon powder for methanol and ethanol electro-oxidation in acid media via cyclic voltammetry and potentiostatic experiments. The supported core–shell nanoparticles have been synthesized by a two-step preparation method that involves a galvanic replacement reaction and characterized by different physico-chemical techniques. The results has been compared with those obtained using a commercial Pt–Ru/C catalyst.

2. Experimental section

Pretreated Vulcan XC-72 R carbon black (S_{BET} = 241 m^2 g^{-1}, and d_p = 40 nm) was used as substrate. The carbon pretreatment was carried out in 5 M HNO_3 solution at 60 °C for 3 h. The slurry was then cooled and its pH value was adjusted to 7.0 with 0.5 M NaOH solution. The pretreated carbon powder was then filtered, washed with water and dried in an oven at 60 °C overnight.

The Cu@Pt–Ru/C catalysts were synthesized via a two-step route. First, copper nanoparticles supported on the pretreated carbon were formed by reduction of the metal precursor with $NaBH_4$ in a buffered aqueous medium at room temperature. A given quantity of $CuSO_4$ was dissolved into a sodium citrate/citric acid buffer solution (pH = 3) under vigorous stirring, and then, a predetermined amount of the pretreated carbon material was added. After 45 min ultrasonic mixing, the metal precursor was reduced by adding solid $NaBH_4$ to the slurry in a reductant to metal weight ratio of 3:1. The Cu/C material was collected via suction filtration, washed thoroughly with bidistilled water and ethanol and finally dried overnight at 60 °C.

The Cu@Pt–Ru core shell particles were prepared by galvanic displacement reaction of Cu with Pt and Ru. 100 mg of the as-prepared carbon supported Cu material was suspended in 50 ml of the sodium citrate/citric acid buffer solution and sonicated for 30 min. Afterward, appropriate amounts of $H_2PtCl_6 \cdot 6H_2O$ and $RuCl_3 \cdot 3H_2O$ aqueous solutions were added and left to react for 2 h under magnetic stirring. The solid product that remained at the end of the reaction was recovered via suction filtration, washed with water and ethanol and dried in an oven overnight. Table 1 lists the specification of all Cu@Pt–Ru core–shell catalysts, with varying platinum loadings (samples Cu(1)–Cu(4)).

The core–shell catalysts were characterized using scanning electronic microscopy (SEM, EVO 40 LEO) and transmission electronic microscopy (TEM, JEOL, 100CX II). X-ray diffraction (XRD) patterns of the catalysts were recorded using a Rigaku Dmax III C diffractometer with monochromated CuKa radiation source operated at 40 keV at a scan rate of 0.05° s^{-1}. Bulk composition analysis was performed by an energy dispersive X-ray (EDX) probe attached to a SEM microscope (JEOL 100). Whereas, the amount of the metals deposited on the carbon substrate was estimated using ICP-AES (Shimadzu 1000 model III). The samples were prepared

Table 1 – Composition and characteristic parameters of Cu@Pt–Ru/C and commercial Pt–Ru/C catalysts.

Catalyst	[a]Pt (wt.%)	[b]Pt (at.%)	[b]Ru (at.%)	[b]Cu (at.%)	[c]d_p(nm)	[d]S_w(m^2 g^{-1}_{Pt-Ru})
Cu(1)	6.4	68.0	2.0	30.0	2.7	67.7
Cu(2)	9.0	77.5	2.0	20.5	2.7	65.1
Cu(3)	11.3	69.5	2.0	28.5	2.4	67.5
Cu(4)	15.0	74.5	2.0	23.5	2.4	67.4
Commercial	20.0	51.0	49.0	–	2.9	60.3

[a] Platinum loading on carbon determined by ICP-AES.
[b] Atomic composition determined by EDX and ICP-AES.
[c] Mean particle size from TEM.
[d] Electroactive surface area per unit mass determined from Cu-UPD and ICP-AES analysis.

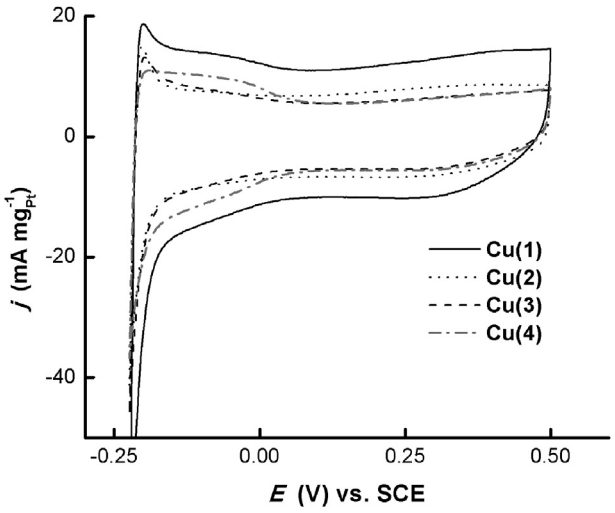

Fig. 1 – Steady cyclic voltammograms of the different carbon supported Cu@Pt–Ru core–shell catalysts in 0.5 M H_2SO_4 at room temperature. υ = 50 mV s^{-1}.

by digesting the supported catalysts in boiling aqua regia and then removing excess acid. The Pt–Ru–Cu electrocatalysts are hereafter designated as Cu(1), Cu(2), Cu(3) and Cu(4) and contain 6.4, 9.0, 11.3 and 15.0 wt.% Pt in carbon.

Conventional three-compartment glass cells were used to run the electrochemical experiments at room temperature with a PAR 273 potentiostat/galvanostat. The counter electrode was a platinum wire separated from the working electrode compartment by a porous glass diaphragm. The reference electrode was a saturated calomel electrode (SCE, +0.241 V vs. RHE) located in a Luggin capillary. The potentials mentioned in this work are referred to this electrode. The working electrode was prepared by dispersing 20 μl of catalyst ink over the surface of a polished glassy carbon rod (3 mm diameter). After that, the electrodes were dried at 60 °C for 30 min to ensure the catalyst binding to the glassy carbon support. The catalyst ink (1 mg/ml) was prepared as follows: 5 mg of catalyst was dispersed in 3.98 ml of bidistilled water, 1 ml of isopropyl alcohol and 20 μl of Nafion® solution (5 wt. %) by sonication for 30 min. Electrochemical techniques such as cyclic voltammetry (CV) and chronoamperometry (CA) were used to characterize the catalysts. All solutions were deaerated by bubbling N_2 for 30 min and then the inert atmosphere was maintained over the solution during the tests. The CV experiments were conducted in 0.5 M H_2SO_4 at a scan rate of 50 mV s^{-1} between 0 and 0.5 V. The stable voltammograms were obtained after 40 cycles. The active surface area of the electrocatalysts was estimated by copper underpotential deposition (Cu-UPD). Experimental details have been described in a previous paper [29]. The electrode activity for the alcohols electro-oxidation was measured in 1 M MeOH or 1 M EtOH + 0.5 M H_2SO_4 solution by applying a potential sweep at a scan rate of 50 mV s^{-1}. Stationary measurements (chronoamperometry) were performed applying pulses from an initial potential of 0 V for 15 min. Current densities for methanol and ethanol electro-oxidation were normalized per milligram of Pt. A commercial Pt–Ru/C electrocatalyst (20 wt.% Pt and 10 wt.% Ru loading, Sigma Aldrich) was used for comparison.

3. Results and discussion

Fig. 1 shows the cyclic voltammetry curves for the different Cu@Pt–Ru/C catalysts in absence of alcohols. The voltammograms did not display a well defined hydrogen adsorption/desorption zone. This behavior is usually observed in carbon supported catalysts decorated with Pt-based nanometric particles [5,6,30]. Some experiments were conducted by setting the anodic limit to 1 V to evaluate the stability of the core–shell systems (figure not shown). The voltammograms obtained after several sweeps exhibited no modifications. On the other hand, we did not observe any anodic/cathodic peaks or waves associated with the dissolution of bulk and/or UPD copper atoms during the potential cycling [28]. The latter strongly suggest that the nanoparticles have a core–shell structure with a Pt-enriched surface region surrounding a Cu-rich alloy core, which in turn prevents the oxidation of Cu to Cu^{2+}.

The composition of all Cu@Pt–Ru catalysts was determined by the EDX technique and ICP-AES analysis (Table 1).

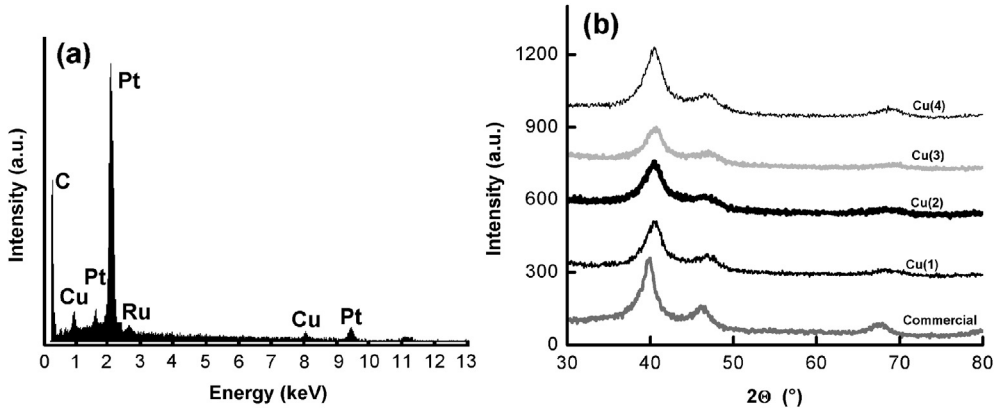

Fig. 2 – XRD patterns of catalysts (a) and EDX spectra of Cu(4) core–shell material.

Fig. 2a shows the typical EDX spectrum of the as-prepared Cu(4) core–shell catalyst. It was determined that the EDX composition for all the samples is very close to that measured by ICP-AES analysis. On the other hand, the proportion of deposited ruthenium to platinum is not within the expected order, taking into account the mol ratio of $RuCl_3$ concentration to H_2PtCl_6 concentration in the solutions. Although the cause of this deviation is not fully understood, it would appear that the galvanic replacement of Cu atoms by Pt^{4+} ions is faster than the replacement of Cu by Ru^{3+} ions.

The XRD diffraction patterns for each core–shell Cu@Pt–Ru/C catalyst are shown in Fig. 2b. For the sake of comparison, the pattern of commercial Pt–Ru/C catalyst is also shown in this figure. The diffractograms of the as-prepared catalysts exhibit the typical features of the face centered cubic (fcc) phase of platinum with the planes (111), (200) and (220) at 2θ values of about 40°, 46° and 69°, respectively. These three diffraction peaks appear slightly shifted toward higher 2θ values in the core–shell materials with respect to the corresponding peaks in a Pt/C catalyst (not shown). Such displacement constitutes an evidence of the incorporation of both Cu and Ru atoms into the fcc structure of Pt and confirms the formation of a solid solution. Besides, no Cu peaks can be observed in the diffractograms of all Cu@Pt–Ru/C systems, suggesting that the nanoparticles are composed of a Pt–Cu-rich alloy core surrounded by a Pt–Ru alloy shell [31]. This behavior has been also observed in PdCu@Pt [32] and Au@Ag [33] core–shell nanoparticles. As was noted by Shibata et al. [33], for small nanoparticles (<4.6 nm) the metals are randomly distributed within the particle due to the interdiffusion across the core–shell interface. However, the interdifussion is limited to the sub interface layers of the nanoparticles and depends on both the core size and the total particle size. Otherwise, large nanoparticles maintain the core–shell structure and interdifussion occurs only in the first monolayer.

The peak profiles in XRD patterns of the catalysts were fitted with the pseudo-Voigt function, using non-linear least-squares refinement procedures based on a finite difference Marquardt algorithm. Using the peak (111) of the fcc structure,

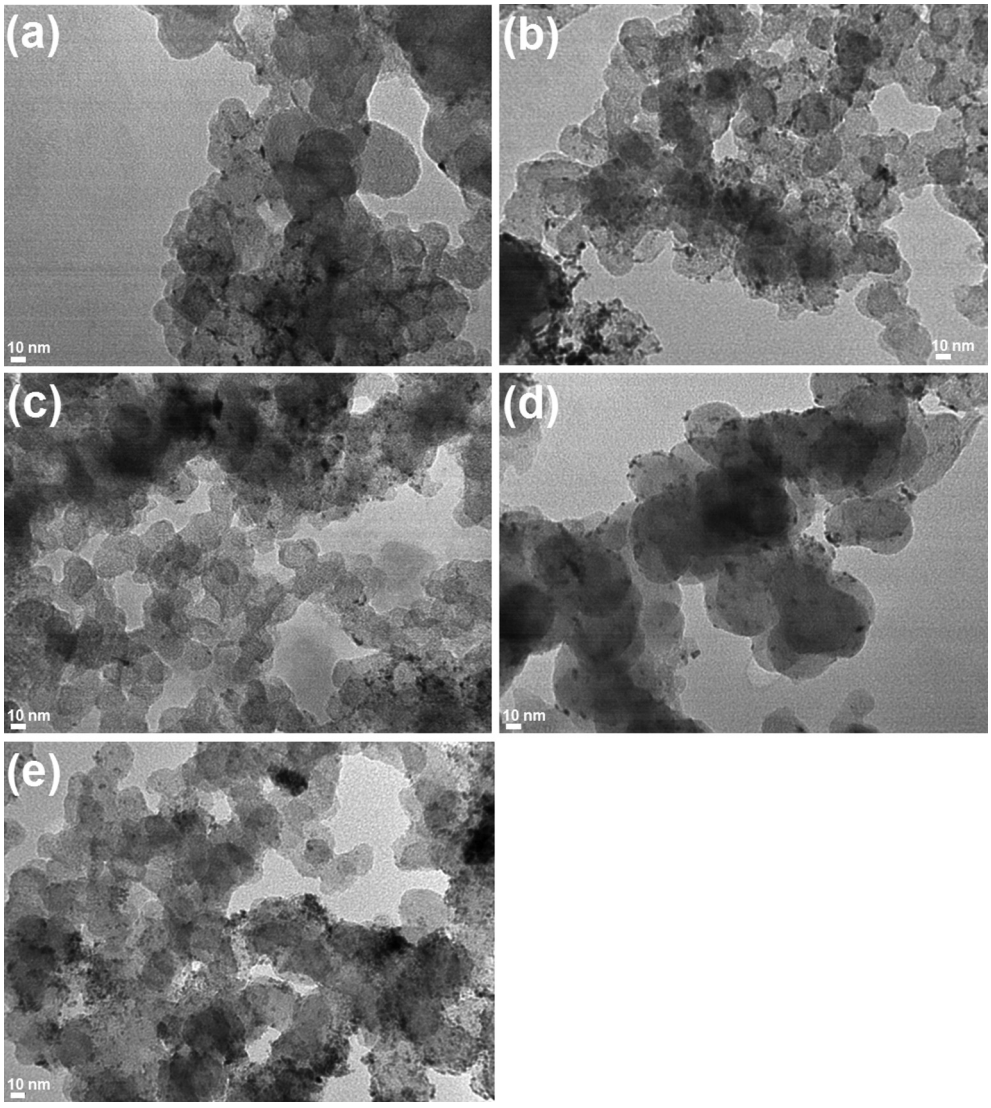

Fig. 3 – TEM images of all materials used in this work. Cu@Pt–Ru/C coreeshell catalysts: Cu(1) (a), Cu(2) (b), Cu(3) (c) and Cu(4) (d), and commercial Pt–Ru/C catalyst (e).

which is not influenced by the broad peak of the carbon support located at a 2θ value of about 26° (not shown), the lattice parameters were estimated using Bragg's law. The lattice parameter (a_{fcc}) values of Cu(1), Cu(2), Cu(3) and Cu(4) were assessed to be 3.853, 3.852, 3.840 and 3.912 Å respectively, while the lattice constant of the commercial catalyst was determined to be 3917 Å. As already noted, the lattice parameter values increase with increasing the Pt content in the samples. In other words, the incorporation of Cu, which has a smaller atomic radius than Pt (1.45 Å against 1. 77 Å), induces the contraction of the Pt fcc network upon alloying, leading consequently to a decrease in the lattice constant.

Additionally Debye-Scherrer's equation [34] was used to estimate the average crystallite size of Cu@Pt–Ru/C and Pt–Ru/C catalysts from the most distinct peak, Pt (111) centered at 2θ values between 39.8 and 40.7°:

$$d_c = \frac{0.94\lambda_{K\alpha 1}}{B_{2\theta}\cos\theta_B} \quad (1)$$

where, $\lambda_{K\alpha 1}$ is the wavelength of X-ray, θ_B is the angle of (111) peak, and $B_{(2\theta)}$ is the full width at half-maximum (FWHM) of the peak broadening in radians and the value 0.94 comes from considering spherical crystallite geometry (cubo-octahedral shape). The average crystallite size of the Cu@Pt–Ru catalysts falls in the range of 2.5–3.0 nm. Furthermore, the commercial Pt–Ru/C catalyst has a crystallite diameter of 3.0 nm.

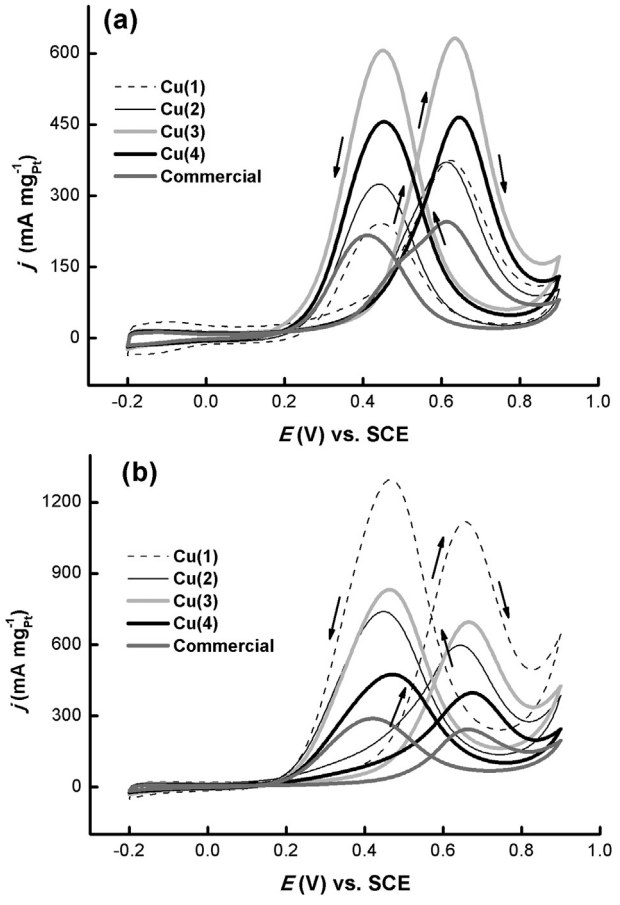

Fig. 4 – Cyclic voltammograms (thirtieth cycle) for the different electrodes in 1 M CH_3OH/0.5 M H_2SO_4 (a), and 1 M CH_3CH_2OH/0.5 M H_2SO_4 (b) at room temperature. The sweep rate was 50 mV s^{-1} and the arrows indicate the scan direction.

Fig. 3 shows the typical TEM images of Cu@Pt–Ru/C core–shell catalysts (Fig. 3a–d) and Pt–Ru/C (Fig. 3e). The TEM images of the as-prepared catalysts reveal the presence of a large amount of nanoparticles which exhibit uniform size and irregular shape with sizes in the range of 2.4–2.7 nm (Table 1). Fig 3 also depicts that the commercial bimetallic catalyst and the core–shell materials have similar particle size, morphology and distribution. However, the as-prepared catalysts exhibit less particle agglomeration than Pt–Ru/C. This result is a direct consequence of the two-step preparation method of the core–shell systems. In the second step, the dissolution of the outermost surface copper and deposition of platinum and ruthenium on the remaining Cu nanoparticles inhibits to a great extent the formation of agglomerates.

In addition, from Table 1 it can be also seen that the electroactive surface area per unit mass (S_w) are only slightly affected by the increase of Pt loading in the core–shell catalysts, indicating that Pt utilization decreases from Cu(1) to Cu(4). Hence, no appreciable modification in the particle size and S_w with variation of Pt content was observed, allowing us to exclude particle size as influential parameter in the electrocatalytic performance of the electrodes. Furthermore, the electroactive surface area of the as-prepared catalysts is higher than that informed for Pt–Ru/C (Table 1). This result can be related to the smaller particle diameter, along with the lower agglomeration degree of Cu@Pt–Ru/C catalysts.

Fig. 4 shows the steady cyclic voltammetry curves recorded for (a) methanol and (b) ethanol electro-oxidation at the as-prepared Cu@Pt–Ru/C and commercial Pt–Ru/C electrodes at room temperature. Current densities for the alcohols electro-oxidation are normalized per milligram of Pt. The shape of curves is characteristic for the electro-oxidation reactions of simple organic alcohols over Pt-based catalysts, showing one anodic peak in the forward scan and one oxidation peak in the backward scan, which is attributed to the oxidative removal of incompletely oxidized carbonaceous species formed in the forward scan and strongly adsorbed on the Pt sites. After reaching a maximum in the forward scan the current decays continuously, and then starts to increase again at potentials higher than 0.8 V due to the formation of incomplete oxidation products [6].

The oxidation of methanol begins at about 0.25 V for all as-prepared catalysts. Interestingly, this onset potential is very similar to that of the commercial Pt–Ru/C material. This means that the incorporation of Cu with Pt plays an important role for improving the CO tolerance of the Pt–Ru shell. The CVs point out that Cu(3) has the greatest activity for methanol oxidation and the intensity of the anodic current during the forward scan is decreased by the order of Cu(4), Cu(2), Cu(1) and Pt–Ru/C. The electrodes effectiveness on methanol conversion to CO_2 can be evaluated in terms of the ratio of the forward peak current density (j_{pf}) to reverse peak current density (j_{pb}). The j_{pf}/j_{pb} value is almost identical for all electrodes, suggesting that the tolerance to CO poisoning of Cu@Pt–Ru/C core–shell materials is comparable with that of the commercial Pt–Ru/C catalyst.

In addition, current transient measurements at constant potentials were carried out for 900 s. The results are summarized in Fig. 5a. As it can be seen, the different electrodes present the same behavior as that observed in the voltammetric curves, but with lower current densities due to the partial blocking of the active sites by the accumulation of the poisoning species due to different reaction and diffusion rates [7,35]. In addition, methanol oxidation current increases when the potential becomes more positive, but then decays due to the low CO_{ads} oxidation rate at the catalyst nanoparticles [36]. As noted above, the catalyst Cu(3) prevails as the best catalyst for the electro-oxidation of the alcohol, followed by Cu(4), Cu(2) and Cu(1), in order of decreasing activity. However, the catalytic activity of Cu(2) and Cu(1) is surpassed by Pt–Ru/C at potentials lower than 0.4 V. Interestingly, the performance of Cu(3) is greater than that of Cu(4) even though the last electrode has higher platinum loading. Ahn et al. [37] have reported that the catalytic activity of core–shell Co–Ru–Pt carbon supported materials increases with the Pt surface molar concentration. The enhancement in catalytic activity was attributed to an increase in the amount of adsorbed carbon monoxide on Pt shell as the surface concentration of Pt increases. This discrepancy can be explained by considering

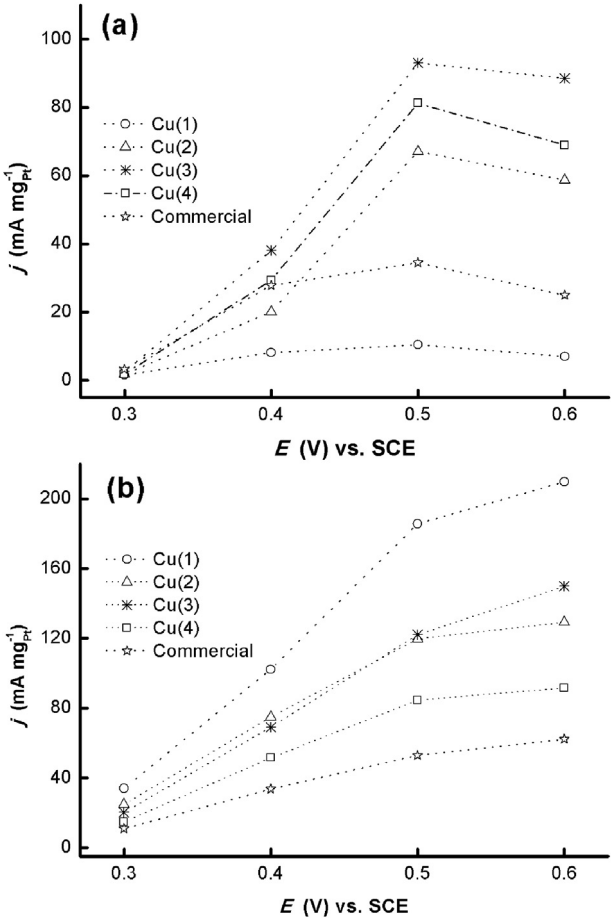

Fig. 5 – Electrocatalytic performance of the electrocatalysts in M CH_3OH/0.5 M H_2SO_4 (a), and 1 M CH_3CH_2OH/0.5 M H_2SO_4 (b). Data taken from chronoamperometry experiments at various potentials after 15 min.

that the activity of the core–shell catalysts also depends strongly on Cu content in the core. Xu et al. [26] have acknowledged that the bimetallic ratio in the sub-layer core should be partly responsible for the catalytic performance of a core–shell system. It is also interesting to note that the catalytic activity of Cu(3) is almost twice higher than that of Cu(1), even when they have similar bulk composition, particle size and electroactive surface area. This may be due to the higher concentration of Pt on the surface of Cu(3) compared to that on Cu(1).

On the other hand, the onset of ethanol oxidation for the as-prepared catalysts is shifted about 0.05 V to more negative potential values than those observed for MeOH oxidation, while the oxidation reaction starts at about 0.4 V for Pt–Ru/C (Fig. 4b). Moreover, the tolerance of the as-prepared catalysts to CO poisoning is higher than that of Pt–Ru/C. This means that the Cu-rich core strongly promotes the oxidation reaction of the alcohol by limiting substantially the accumulation of ethanolic residues or favoring the splitting of the C–C bond. Furthermore, it could be seen that the catalytic activities (current densities) for EtOH oxidation were higher than that observed for MeOH oxidation. This behavior may be related to the difference in their adsorption behavior on the catalyst surfaces at the potential region between 0.2 and 0.4 V [38]. As can be clearly observed in Fig. 5b the different electrodes present the same behavior as that viewed in the voltammetric curves, but with lower current densities. In this case, the best performance for the electro-oxidation of the alcohol was obtained with Cu(1) and decreased in the order of Cu(2) > Cu(3) > Cu(4) > Pt–Ru/C, although the catalytic activity of Cu(3) exceeds that of Cu(2) for potentials above 0.5 V. Conversely to methanol reaction, the catalytic activity towards ethanol oxidation decreases as the platinum loading is increased. The reason for such behavior may have to do with Cu content in the particle core. Because a richer Cu core induces more lattice-strain in the shell, the compression of the lattice parameter can favor the splitting of the C–C bond or reduce the binding energy of intermediates, improving EtOH utilization and consequently the performance of the catalysts. The C–C bond cleavage is known to be sensitive to specific geometric arrangements of the surface metal atoms, which in turns affects parameters as bond length and angles [39]. This behavior has been observed by several authors, both experimentally and theoretically, for the oxygen reduction reaction [17,40,41].

The superior performance of the as-prepared core–shell Cu@Pt–Ru catalysts with respect to the commercial Pt–Ru/C material can be ascribed to the modification of the surface electronic structure (changes in the density of states near the Fermi level) due to lattice-strain and surface ligand effects [40,42]. In other words, the lattice mismatch between the Pt-rich shell and the Pt–Cu-rich core reduce the interatomic distance in the shell, this effect shift the d-band and, thus, influence the Pt–CO_{ads} binding energy [16,17,43,44]. Moreover, the lattice compression may develop a large number of surface defect sites such as step edges and kinks, which exhibit very high catalytic activity for methanol and ethanol oxidation [45]. In addition, the lower agglomeration degree of Cu@Pt–Ru/C can also contribute in some extent to their higher catalytic activity towards methanol and ethanol

oxidation. Future work will be focus on the preparation and characterization of core–shell systems of low Pt loading (<10 wt.%) with higher ruthenium content and as well as the direct application of these catalysts in membrane electrode assemblies (MEAs).

4. Conclusion

In this paper core–shell Cu@Pt–Ru supported catalysts have been successfully synthesized by a two-step process that involves a galvanic replacement reaction. The as-prepared catalysts exhibit particles with sizes in the range of 2.4–2.7 nm homogeneously distributed over the carbon support. CVs experiments, XRD and EDX analysis suggests the presence of a Pt–Cu-rich core surrounded by a Pt-rich shell. Both potentiodynamic and potentiostatic measurements showed that the as-prepared core–shell electrocatalysts display superior catalytic activity towards methanol and ethanol electrooxidation compared to a commercial Pt–Ru/C material with higher Pt loading. The latter was attributed to the lattice mismatch between the Pt-rich shell and the Pt–Cu-rich core, which produce lattice-strain and modification of the electronic surface structure. Besides, the development of a large amount of surface defect sites can contribute to the better performance of Cu@Pt–Ru materials.

Acknowledgments

This work was supported by ANPCYT grant PICT-438. The authors are grateful to Graciela Mas for her assistance in the XRD measurements. V. Comignani thanks the CONICET for a Ph.D. fellowship.

REFERENCES

[1] Léger JM, Coutanceau C, Lamy C. Electrocatalysis for the direct alcohol fuel cell. In: Koper MTM, editor. Fuel cell catalysis: a surface science approach. New Yersey: John Wiley & Sons; 2009. pp. 343–74.
[2] Eggert RG. Minerals go critical. Nat Chem 2011;3:688–91.
[3] Vielstich W, Lamm A, Gasteiger HA. Handbook of fuel cells: fundamentals, technology and applications, vol. 2. New York: John Wiley & Sons; 2003.
[4] Kakaç S, Pramuanjaroenkij A, Vasiliev L. Mini-micro fuel cells: fundamentals and applications. The Netherlands: Springer; 2008.
[5] Cunha EM, Ribeiro J, Kokoh KB, de Andrade AR. Preparation, characterization and application of Pt-Ru-Sn/C trimetallic electrocatalysts for ethanol oxidation in direct fuel cell. Int J Hydrogen Energy 2011;36:11034–42.
[6] Sieben JM, Duarte MME. Methanol, ethanol and ethylene glycol electro-oxidation at Pt and Pt-Ru catalysts electrodeposited over oxidized carbon nanotubes. Int J Hydrogen Energy 2012;37:9941–7.
[7] Sieben JM, Duarte MME. Nanostructured Pt and Pt-Sn catalysts supported on oxidized carbon nanotubes for ethanol and ethylene glycol electrooxidation. Int J Hydrogen Energy 2011;36:3313–21.
[8] Tsiakaras PE. PtM/C (M = Sn, Ru, Pd, W) based anode direct ethanol-PEMFCs: structural characteristics and cell performance. J Power Sources 2007;171:107–12.
[9] Zhou W, Zhou Z, Song S, Li W, Sun G, Tsiakaras P, et al. Pt based anode catalysts for direct ethanol fuel cells. Appl Catal B 2003;46:273–85.
[10] Kadirgan F, Kannan AM, Atilan T, Beyhan S, Ozenler SS, Suzer S, et al. Carbon supported nano-sized Pt-Pd and Pt-Co electrocatalysts for proton exchange membrane fuel cells. Int J Hydrogen Energy 2009;34:9450–60.
[11] Lopes T, Antolini E, Gonzalez ER. Carbon supported Pt-Pd alloy as an ethanol tolerant oxygen reduction electrocatalyst for direct ethanol fuel cells. Int J Hydrogen Energy 2008;33:5563–70.
[12] Zhu H, Liu Y, Shen L, Wei Y, Guo Z, Wang H, et al. Microwave heated polyol synthesis of carbon supported PtAuSn/C nanoparticles for ethanol electrooxidation. Int J Hydrogen Energy 2010;35:3125–8.
[13] Shen SY, Zhao TS, Xu JB. Carbon supported PtRh catalysts for ethanol oxidation in alkaline direct ethanol fuel cell. Int J Hydrogen Energy 2010;35:12911–7.
[14] Hoster HE, Iwasita T, Baumgrtner E, Vielstich W. Pt-Ru model catalysts for anodic methanol oxidation: influence of structure and composition on the reactivity. Phys Chem Chem Phys 2001;3:337–46.
[15] Wang JX, Inada H, Wu L, Zhu Y, Choi YM, Muller DA, et al. Oxygen reduction on well-defined core-shell nanocatalysts: particle size, facet, and Pt shell thickness effects. J Am Chem Soc 2010;132:17664–6.
[16] Wang D, Xin HL, Yu Y, Wang H, Rus E, Muller DA, et al. Pt-decorated PdCo@Pd/C core-shell nanoparticles with enhanced stability and electrocatalytic activity for the oxygen reduction reaction. J Am Chem Soc 2009;131:17298–302.
[17] Strasser P, Koh S, Anniyev T, Greeley J, More K, Yu C, et al. Lattice-strain control of the activity in dealloyed core-shell fuel cell catalysts. Nat Chem 2010;2:454–60.
[18] Wang L, Yamauchi Y. Autoprogrammed synthesis of triple-layered Au@Pd@Pt core-shell nanoparticles consisting of a Au@Pd bimetallic core and nanoporous Pt shell. J Am Chem Soc 2010;132:13636–8.
[19] Shao M, Shoemaker K, Peles A, Kaneko K, Protsailo L. Pt monolayer on porous Pd-Cu alloys as oxygen reduction electrocatalysts. J Am Chem Soc 2010;132:9253–5.
[20] Chen TY, Luo TJM, Yang YW, Wei YC, Wang KW, Lin TL, et al. Core dominated surface activity of core–shell nanocatalysts on methanol electrooxidation. J Phys Chem C 2012;116:16969–78.
[21] Jiang X, Gür TM, Prinz FB, Bent SF. Atomic layer deposition (ALD) Co-deposited Pt-Ru binary and Pt skin catalysts for concentrated methanol oxidation. Chem Mater 2010;22:3024–32.
[22] Karan HI, Sasaki K, Kuttiyiel K, Farberow CA, Mavrikakis M, Adzic RR. Catalytic activity of platinum monolayer on iridium and rhenium alloy nanoparticles for the oxygen reduction reaction. ACS Catal 2012;2:817–24.
[23] Xing Y, Cai Y, Vukmirovic MB, Zhou WP, Karan H, Wang JX, et al. Enhancing oxygen reduction reaction activity via PdAu alloy sublayer mediation of Pt monolayer electrocatalysts. J Phys Chem Lett 2010;1:3238–42.
[24] Gong K, Su D, Adzic RR. Platinum-monolayer shell on $AuNi_{0.5}Fe$ nanoparticle core electrocatalyst with high activity and stability for the oxygen reduction reaction. J Am Chem Soc 2010;132:14364–6.
[25] Yan S, Zhang S. Methanol electrooxidation on carbon supported Aucore-Ptshell nanoparticles synthesized by an epitaxial growth method. Int J Hydrogen Energy 2012;37:9636–44.

[26] Xu C, Liu Y, Wang J, Geng H, Qiu H. Fabrication of nanoporous Cu-Pt(Pd) core/shell structure by galvanic replacement and its application in electrocatalysis. Appl Mater Interfaces 2011;3:4626–32.
[27] Kaplan D, Burstein L, Rosenberg Y, Peled E. Comparison of methanol and ethylene glycol oxidation by alloy and core–shell platinum based catalysts. J Power Sources 2011;196:8286–92.
[28] Ammam A, Easton EB. PtCu/C and Pt(Cu)/C catalysts: synthesis, characterization and catalytic activity towards ethanol electrooxidation. J Power Sources 2013;222:79–87.
[29] Sieben JM, Duarte MME, Mayer CE. Supported Pt and Pt–Ru catalysts prepared by potentiostatic electrodeposition for methanol electrooxidation. J Appl Electrochem 2008;38:483–90.
[30] Mani P, Srivastava R, Strasser P. Dealloyed Pt-Cu core-shell nanoparticle electrocatalysts for use in PEM fuel cell cathodes. J Phys Chem C 2008;112:2770–8.
[31] Sarkar A, Manthiram A. Synthesis of Pt@Cu core-shell nanoparticles by galvanic displacement of Cu by Pt4+ ions and their application as electrocatalysts for oxygen reduction reaction in fuel cells. J Phys Chem C 2010;114:4725–32.
[32] Cochell T, Manthiram A. Pt@PdxCuy/C Core–Shell electrocatalysts for oxygen reduction reaction in fuel cells. Langmuir 2012;28:1579–87.
[33] Shibata T, Bunker BA, Zhang Z, Meisel D, Vardeman CF, Gezelter JD. Size-dependent spontaneous alloying of Au-Ag nanoparticles. J Am Chem Soc 2002;124:11989–96.
[34] Warren BE. X-ray diffraction. Reading, Massachusetts: Addison-Wesley; 1969.
[35] Hamnett A. In: Wieckowski A, editor. Interfacial electrochemistry. New York: Marcel Dekker; 1999. p. 843.
[36] Cherstiouk OV, Simonov PA, Savinova ER. Model approach to evaluate particle size effects in electrocatalysis: preparation and properties of Pt nanoparticles supported on GC and HOPG. Electrochim Acta 2003;48:3851–60.
[37] Ahn SH, Choi I, Kwon OJ, Lim T, Kim JJ. Electrochemical preparation of Pt-based catalysts on carbon paper treated with Sn sensitization and Pd activation. Int J Hydrogen Energy 2012;37:41–50.
[38] Gootzen JFE, Wonders AH, Cox AP, Visscher W, van Veen JAR. On the adsorbates formed during the platinum catalyzed (electro)oxidation of ethanol, 1,2-ethanediol and methyl-α-image-glucopyranoside at high pH. J Mol Catal A: Chem 1997;127:113–31.
[39] Schauermann S, Hoffmann J, Johánek V, Hartmann J, Libuda J, Freund HJ. Catalytic activity and poisoning of specific sites on supported metal nanoparticles. Angew Chem Int Ed 2002;41:2532–5.
[40] Wang D, Xin HL, Wang H, Yu Y, Rus E, Muller DA, et al. Facile synthesis of carbon-supported Pd-Co core-shell nanoparticles as oxygen reduction electrocatalysts and their enhanced activity and stability with monolayer Pt decoration. Chem Mater 2012;24:2274–81.
[41] Kettner M, Schneider WB, Auer AA. Computational study of Pt/Co core-shell nanoparticles: segregation, adsorbates and catalyst activity. J Phys Chem C 2012;116:15432–8.
[42] Stamenkovic VR, Mun BS, Mayrhofer KJJ, Ross PN, Markovic NM. Effect of surface composition on electronic structure, stability, and electrocatalytic properties of Pt-transition metal alloys: Pt-skin versus Pt-skeleton surfaces. J Am Chem Soc 2006;128:8813–9.
[43] Nilekar AU, Alayoglu S, Eichhorn B, Mavrikakis M. Preferential CO oxidation in hydrogen: reactivity of core-shell nanoparticles. J Am Chem Soc 2010;132:7418–28.
[44] Koenigsmann C, Santulli AC, Gong K, Vukmirovic MB, Zhou W, Sutter E, et al. Enhanced electrocatalytic performance of processed, ultrathin, supported Pd-Pt core-shell nanowire catalysts for the oxygen reduction reaction. J Am Chem Soc 2011;133:9783–95.
[45] Savinova ER, Hahn F, Alonso-Vante N. The assessment of nanocrystalline surface defects on real versus model catalysts probed via vibrational spectroscopy of adsorbed CO. Surf Sci 2009;603:1892–9.